Reaction Chemistry & Engineering

ROYAL SOCIETY OF CHEMISTRY

PAPER

View Article Online
View Journal | View Issue

Cite this: *React. Chem. Eng.*, 2021, **6**, 709

Using design of experiment to obtain a systematic understanding of the effect of synthesis parameters on the properties of perovskite nanocrystals†

Robert W. Baker,*[ab] Laura Forfar,[c] Xinxing Liang[b] and Petra J. Cameron *[ab]

Received 17th April 2020,
Accepted 17th February 2021

DOI: 10.1039/d0re00149j

rsc.li/reaction-engineering

Lead halide perovskite nanocrystals have emerged as promising materials for optoelectronic applications. Their properties can be tuned by changing the synthesis conditions, but usually these conditions are studied in isolation rather than holistically. We report the use of design of experiment in the synthesis of $MAPbI_3$ nanocrystals. Eight factors were investigated in a broad screening study; we then focussed on five factors in a more refined screening study that targeted desired optoelectronic properties. An empirical model was developed and validated proving that five factors could be understood within a low number of experiments. By controlling the reactant solvent ratio, ligand concentration, ligand ratio, non-polar solvent polarizability, and purification solvent, the $MAPbI_3$ photoluminescence peak position could be tuned from 614 to 737 nm. The model has provided greater insight into the nanocrystal morphology and stability.

Introduction

Research into lead halide perovskites has grown rapidly since 2012[1] largely due to the impressive efficiencies of perovskite photovoltaics. The power conversion efficiency of perovskite solar cells has reached 25.5%, which is comparable to silicon PV devices.[2] Lead halide and related perovskites are also finding applications in light emitting diodes (LEDs),[3] lasers[4] and photodetector research.[5] More recently, interest has grown in perovskite nanocrystals (NCs). Halide substitution of the NCs allows the band gap to be tuned across the visible spectrum with narrow photoluminescence (PL) peak widths (12–42 nm) and high photoluminescence quantum yields (PLQY). One of the most studied materials, $CsPbX_3$, where X = I or Br has quantum yields exceeding 90%.[6]

Perovskite NCs are usually synthesized at high temperatures, typically 150–200 °C in batch using a process called hot injection.[7–9] Batch methods can suffer from issues with batch to batch reproducibility and are difficult to scale up to meet industrial demand.[10] Furthermore, synthesis cost has been noted to be critical in the commercial viability of nanocrystal PVs.[11] One method to reduce costs is to synthesise the NCs at room temperature through ligand assisted reprecipitation (LARP).[12–14] This method, however, produces a lot of bulk material and is again typically done in batch.

A third synthesis method is continuous production through the use of microfluidic flow synthesis.[15] Microfluidic flow synthesis can be a cost effective way to produce high quality NCs continuously and avoids challenges with scaling up batch reactors. Furthermore, conditions can be changed and monitored in real time though inline analysis.[16] de Mello's group have made substantial progress in synthesizing $FAPbX_3$,[17] $Cs_xFA_{1-x}Pb(Br_{1-y}I_{y3})_3$,[18] and $FAPb(Cl_{1-x}Br_x)_3$,[19] NCs using microfluidics at high temperatures. Our group has demonstrated room temperature synthesis of $MAPb(Br_{1-x}I_x)_3$ in flow.[20]

Perovskite NCs can be modified by altering the anion and cation ratios to make materials with a range of stoichiometries and material properties. The chosen synthesis conditions such as solvent, ligands and temperature also impact the NCs size and shape.[21–26] Typically these factors are changed by one variable at a time (OVAT) to systematically study the impact on the NCs size, morphology and PL properties. This approach, while very thorough, can be an inefficient use of time and resources, and does not give insight into interactions between variables. Previously, more thorough investigation of reaction conditions in flow synthesis has been achieved by parametric screening[15] and self-optimising Kriging algorithms[27] to quickly screen

[a] *Centre for Sustainable and Circular Technologies, University of Bath, Bath, UK. E-mail: rb894@bath.ac.uk, p.j.cameron@bath.ac.uk*
[b] *Department of Chemistry, University of Bath, Bath, UK*
[c] *Paul Murray Catalysis Consulting Ltd., UK. E-mail: laura.forfar@catalysisconsulting.co.uk; Tel: +44 (0)1454 325530*

† Electronic supplementary information (ESI) available. See DOI: 10.1039/d0re00149j

multiple variables in a single study. These methods, however, demand a large number of experiments and have only focused on a relatively low number of factors such as anion ratio (Br/I), temperature, Pb/Cs ratio[15] and cation ratio (Cs/FA).[27]

The large number of potentially important parameters involved in the synthesis of NCs can be rapidly investigated by employing a statistical technique, design of experiments (DoE). Experimental design, while commonly used in the pharmaceutical industry and analytical chemistry,[28,29] is relatively underused in academia with only a few examples found in the perovskite and PV literature.[30–32]

Experimental

Materials

Lead(II) iodide (PbI_2, 99%), mesitylene (99%), ethyl butanoate (99%) and ethyl acetate (99.5%) were purchased from Sigma Aldrich. Methylammonium iodide (MAI, 99%) was purchased from Greatcell Solar. 1-Butanol (1-BuOH, 99%), 1-octadecene (1-ODE, 90%), oleylamine (OLA, 80–90%) and dodecane (99%) were purchased from Acros Organics. Hexane (reagent grade) and toluene (reagent grade) were purchased from VWR Chemicals. Oleic acid (OA, 90%) and dichloromethane (99%) were purchased from Alfa Aesar. All chemicals was used as received without further purification.

Flow synthesis

As is the nature of a designed experiment, precursor preparation and synthetic conditions were varied in each experiment, however, the general steps are described below. PbI_2 (0.8 mmol, 368.8 mg) was dissolved in 8 mL of the non-polar solvent (1-ODE, dodecane or hexane) with varying concentrations of OA and OLA (in a 1 : 1 ratio). The solution was then stirred and heated to 100 until the precursors had dissolved. MAI (0.8 mmol, 127.2 mg) was dissolved in 12 mL of 1-BuOH and non-polar solvent (1-ODE, dodecane or hexane), with varying ratios, along with OA and OLA. Further details are given in the ESI.†

The flow synthesis used in this study was adapted from our previously reported work.[20] An overview of the process and the factors investigated are shown in Fig. 1. The PbI_2 and MAI precursor solutions were loaded into separate syringes. Syringe pumps were used to inject the solution into a 17 m long 1/16″ O.D. PTFE tube (Kinesis, 0.8 mm I.D) immersed in a water bath between 20–40 °C. The total flow rate was maintained at 0.855 mL min^{-1}, a 10 min residence time. The solution met in either a standard T-junction (P-632, Kinesis) or a mixing T-junction (CM1XKF, Cheminert). The product was collected in a centrifuge tube and centrifuged at 7000 rpm for 10 min. The first supernatant, S1, was retained for analysis and the pellet was resuspended in the appropriate purification solvent (ethyl acetate, ethyl butanoate, dichloromethane, hexane, toluene, mesitylene). The suspension was centrifuged again for 10 min at 7000 rpm and the second supernatant, S2, was retained for analysis.

Characterisation

The photoluminescence of the two supernatant solutions (S1 and S2) was analyzed in a 1 cm quartz cuvette under ambient conditions at 365 nm using a Agilent Technologies Cary Eclipse spectrophotometer and the UV-vis spectra were measured on a Agilent Technologies Cary 60 spectrophotometer. Photoluminescence quantum yields (PLQY) were recorded with reference to zinc phthalocyanine (PLQY = 30%, λ_{ex} = 605 nm) in 1% pyridine/toluene. The optical density of the samples was less than 0.1 to prevent reabsorption and the quantum yields were calculated using eqn (1) where Φ is the quantum yield, grad is the gradient of the integrated fluorescence *vs.* absorbance at the excitation wavelength, and η is the solvent refractive index and x and ST denote the sample and standard respectively.

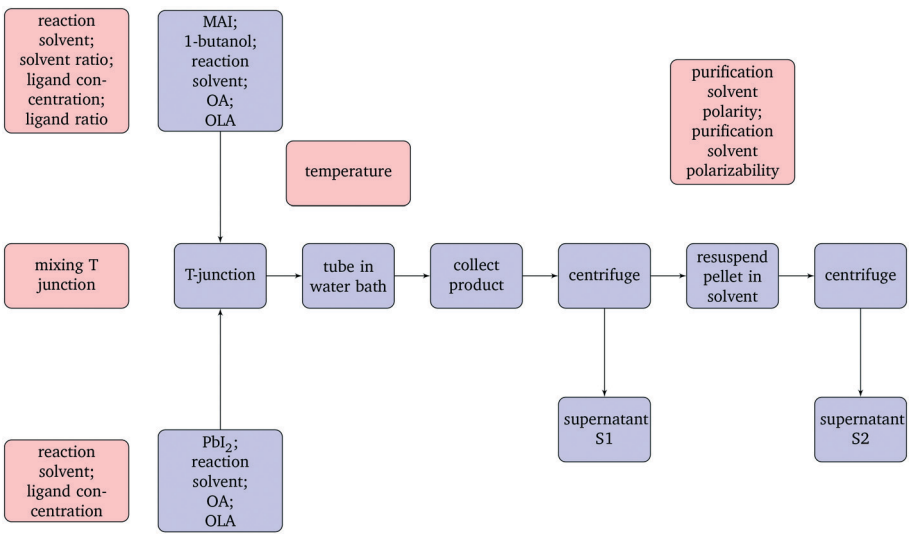

Fig. 1 Flow diagram of the synthesis process (blue) and the factors studied in the design of experiments (red).

$$\Phi_x = \Phi_{ST}\left(\frac{\text{grad}_x}{\text{grad}_{ST}}\right)\left(\frac{{\eta_x}^2}{{\eta_{ST}}^2}\right) \quad (1)$$

Transmission electron microscopy (TEM) samples were prepared on carbon coated copper grids and analysed at a 200 kV acceleration voltage using a JEOL JEM-2100Plus electron microscope. X-ray diffraction (XRD) samples were deposited onto a plastic film and measurements were conducted on a STADI P diffractometer in transmission mode using a Cu Kα source.

Fractional factorial design

A factorial design is a structured set of experiments where the factors (x_i) *e.g.* temperature or ligand concentration, are varied across a specified range *e.g.* 20 °C to 40 °C. The experiments are run at the extremes of the selected ranges ('low' and 'high' value) and at the centre point, rather than explored incrementally as seen in parametric screening.[15] A fractional factorial design (FFD) uses a fraction of the potential combination of factors to reduce the number of experiments, since the number of experiments increases exponentially (2^n) with the number of factors (n) investigated. The responses are the measured output (y), such as PL peak position. Models can be fitted to the data, in these examples using multiple linear regression, to explain which main ($\beta_i x_i$) and interaction terms ($\beta_{ij} x_i x_j$) are contributing to a change in response. Squared terms ($\beta_{ii} {x_i}^2$) may also be necessary to explain a non-linear change in the response. β_0 and ε are the constant coefficient (y-intercept) and the random error respectively.

$$y = \beta_0 + \sum_{i=1}^{k} \beta_i x_i + \sum_{1 \le i \le j}^{k} \beta_{ij} x_i x_j + \sum_{i=1}^{k} \beta_{ii} {x_i}^2 + \varepsilon \quad (2)$$

By removing insignificant terms from eqn (2), empirical models can be constructed which describe the relationship between the factors and the response. These models are then evaluated by four key metrics which are calculated by the DoE software: R^2, Q^2, model validity and model reproducibility values. R^2 describes the overall model fit, how well it describes the data. Q^2 estimates the ability of the model to make predictions within the specified ranges. Model validity indicates whether there are issues with the model such as missing terms. Reproducibility compares the variation of the control experiments to the overall variability of the dataset. Typical values for a good, satisfactory, and a poor model fit can be found in Table S3 in the ESI.†

Broad screening fractional factorial design

Chosen factors and ranges

Previous studies have demonstrated that the reaction temperature,[6] ligand concentration,[33] ligand ratio[34] and ligand chain length,[23] are critical in controlling NC size and dimensions. Other variables such as solvent,[35] and solvent ratios[36] have also been studied. Experimental conditions are most often investigated by changing one variable at a time, while controlling all the other variables. Investigating these parameters using design of experiments will deliver a greater understanding of the whole synthesis, including any interactions between factors.

Before beginning the design, the relevant factors needed to be selected and their ranges established. Fang *et al.* have previously reported nanocrystal synthesis in batch using polar solvent controlled ionisation.[36] The PbX_2 salt was dissolved in 1-octadecene (1-ODE) with an equal ratio of oleic acid and oleylamine. The cation source, caesium oleate, was dissolved in 1-ODE. 1–50% of protic polar solvents were added to ionise the precursors and induce nucleation of the NC particles. In our system, PbX_2 is also dissolved in 1-ODE with oleic acid and oleylamine. The cation source, MAX, is first dissolved in 1-butanol, then 1-ODE and oleic acid are added. The two solutions are then mixed in flow in a T-junction. Fang *et al.* investigated ethanol, isopropanol, 1-butanol, acetone and acetidin as well as oleic acid as suitable polar solvents.

Since these polar solvents are relatively safe and sustainable,[37] in this DoE we chose to look at the effect of replacing the more dangerous and unsustainable non-polar solvents in the synthesis, as sustainable non-polar solvents are of particular interest for commercial scale-up.

Initial results showed that only the most non-polar solvents could be used successfully in the flow synthesis of NCs. However, changing the polarizability of the non-polar solvent had an effect on the NC PL peak position being formed. In these experiments we used ODE, hexane and dodecane. A second parameter chosen for the DoE was the polarity of the solvent used to purify the nanocrystals.[38] It is important to note that the purification solvent polarity was restricted to the non-polar half of the solvent map as polar solvents such as ethanol and DMSO rapidly degrade the NCs.

Other preliminary tests suggested that the ratio of the non-polar reaction solvent to 1-butanol was critical to the quality of the NCs formed. Ligand concentration (ligand : Pb ratio), ligand ratio (% OA to OLA), and temperature were also chosen as factors for investigation. Since the reaction was performed in flow, two different types of T-junctions were investigated to see if the rate of mixing had an effect on the NC nucleation and growth. In total, eight factors were chosen for investigation and their ranges established, according to Table 1. The solvent selection for each reactant and purification solvent is detailed in the ESI† Table S1.

Experimental designs were created and analysed using Modde Pro (version 12.0.1), the exact combination of conditions run are shown in Table 2. The resolution IV fractional factorial design (FFD) consisted of 16 experiments plus three repeats at the centre point (control experiments N17–19). A resolution IV FFD will assess the importance of the factors across the investigated ranges. There is no confounding with the main factors but 2-way interactions are confounded. An absolute

Table 1 Screening design factors and ranges where −1, 0 and 1 are the low, centre and high values which are further explained in the ESI† Table S1

	Factor	Range		
		Low	Centre	High
1	Non-polar solvent/%	50	57.5	65
2	Non-polar solvent polarisability	−1	0	1
3	Ligand concentration (ligand : Pb)	8	13	18
4	Oleic acid/%	50	57.5	65
5	Temperature/°C	20	30	40
6	Mixing	Low		High
7	Purification solvent polarity	−1	0	1
8	Purification solvent polarizability	−1	0	1

characterisation of the interactions is not possible with this design type, but additional experimentation can be used to resolve interactions in more detail.

Responses

With the factors and ranges set, the chosen responses, or the measurable output for each nanoparticle solution synthesized, were the PL peak intensity, peak position and peak width. Usually peak position and the peak width are described by the wavelength at the highest intensity (mode), and the full width at half maximum respectively (FWHM). During the preliminary tests, it was observed that the peaks in some PL spectra were quite asymmetric. In some other spectra multiple peaks were recorded. The mode and the FWHM were therefore not the best metrics to measure in this circumstance. Instead the median wavelength and the interquartile range of the whole PL signal were chosen as more appropriate measures of peak position and peak width respectively. A qualitative examination of the stability of the NC solutions was also noted.

Screening fractional factorial design results

Once the factors had been decided, 19 experiments (16 + 3 centre points) were carried out (as described in Table 2) and the responses recorded. The median of the PL peak and the interquartile range were measured and input into Modde for analysis. The regression model was refined by removing insignificant interactions ($\beta_{ij}x_ix_j$) and insignificant main terms (β_ix_i) from the equation. The coefficient plots for each model, and an explanation of determining significant and insignificant factors can be found in the ESI† (Fig. S2 and S3).

The first set of screening experiments allowed us to draw several conclusions. Firstly, the median of the peak due to PL emission from the as formed NCs varied between 623–736 nm, Fig. 2b. Secondly, the results suggest only the most non-polar solvents were suitable for NC purification. Sample purification in ethyl acetate, ethyl butanoate and dichloromethane led to very dilute solutions which either had very low or high intensities. Some S2 solutions had low NC concentrations so therefore the intensity was low. Other solutions, however, had high intensities due to a reduction in self quenching which was confirmed by diluting a representative S2 sample. As a result, no conclusions could be drawn from the S2 intensity model. Diluting the S1 showed a linear relationship between concentration and fluorescence intensity confirming self-quenching was not present. It is important to emphasise that as the S1 supernatant showed a linear increase in fluorescence intensity with concentration (Fig. S9(a)†), intensity of the S1 solutions was a legitimate measure of NC quality. Thirdly, in experiments N5 to N8 (50% OA, ligand : Pb = 18) NCs were not produced. High ligand concentration at 50% OA prevented the NCs from nucleating and no fluorescence was observed. At 65% OA, the acid : base equilibrium[33] was shifted such that NCs were produced in both high and low ligand concentrations (N9 to N16). Finally, the variation in the PL measured for all control experiments (N17–19) was low therefore

Table 2 Screening design experimental formulations and conditions

Exp no.	Run order	Non-polar solvent/%	Non-polar solvent	Ligand : Pb/mmol : mmol	Oleic acid/%	Temperature/°C	Mixing	Purification solvent
N1	13	50	Hexane	8	50	20	Low	Ethyl acetate
N2	17	65	Hexane	8	50	20	High	Mesitylene
N3	11	50	1-ODE	8	50	40	Low	Mesitylene
N4	16	65	1-ODE	8	50	40	High	Ethyl acetate
N5	14	50	Hexane	18	50	40	High	Hexane
N6	10	65	Hexane	18	50	40	Low	Dichloromethane
N7	3	50	1-ODE	18	50	20	High	Dichloromethane
N8	4	65	1-ODE	18	50	20	Low	Hexane
N9	15	50	Hexane	8	65	40	High	Dichloromethane
N10	5	65	Hexane	8	65	40	Low	Hexane
N11	8	50	1-ODE	8	65	20	High	Hexane
N12	2	65	1-ODE	8	65	20	Low	Dichloromethane
N13	12	50	Hexane	18	65	20	Low	Mesitylene
N14	9	65	Hexane	18	65	20	High	Ethyl acetate
N15	19	50	1-ODE	18	65	40	Low	Ethyl acetate
N16	6	65	1-ODE	18	65	40	High	Mesitylene
N17	7	57.5	Dodecane	13	57.5	30	Low	Ethyl butanoate
N18	18	57.5	Dodecane	13	57.5	30	Low	Ethyl butanoate
N19	1	57.5	Dodecane	13	57.5	30	Low	Ethyl butanoate

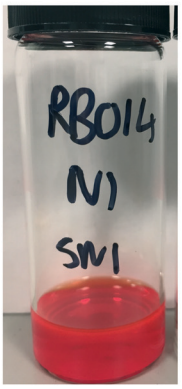

(a) N1

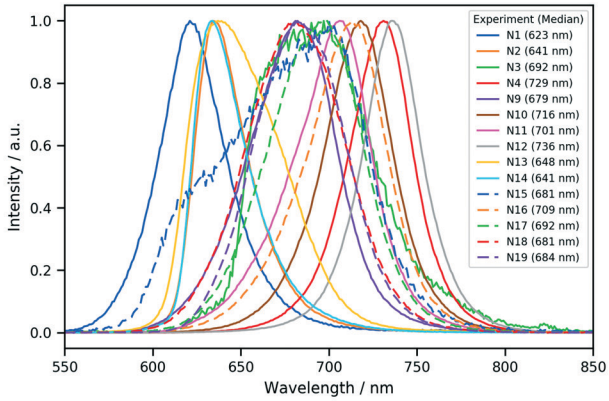

(b) S1 PL emission

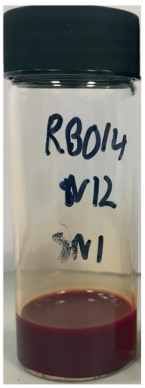

(c) N12

Fig. 2 Broad screening design (a) experiment N1, shortest PL wavelength, (b) S1 normalised PL emission response, and (c) experiment N12, longest PL wavelength.

models could be produced for all the responses except for the S2 intensity response.

Four experiments (N5–8) did not produce NCs and therefore there are no associated values for peak width and intensity. It is difficult to develop a meaningful model from incomplete datasets. Therefore, experiments that did not produce nanocrystals were artificially allocated an interquartile range of 100 nm for peak width, to suggest a very broad and undesirable peak, and an intensity value of 0 since there was no PL emission.

For each response (y) model, the insignificant main terms and interactions were removed from eqn (2) in the regression analysis and the model metrics (R^2, Q^2, model validity and reproducibility) were evaluated. All the response models, except for purified peak width, exhibited good or satisfactory R^2, Q^2 and reproducibility values indicating that the models can be accurately used to explain and predict data within the range investigated. A summary of the model metrics and coefficient plots for each response is shown in the ESI† Table S4.

The initial screening highlighted the importance of the non-polar solvent content and polarisability, ligand concentration and ratio, temperature and purification solvent polarisability, and their impact on the peak position, width and intensity. Using two different mixing T-junctions had no impact in any model. Purification solvent polarity had a large effect on the stability of the S2 NCs solutions. The more polar purification solvents, ethyl acetate and dichloromethane, and the centre point, ethyl butanoate, degraded the perovskite NCs over several days indicating that only very non-polar solvents are suitable for stable colloidal NC solutions. To gain further insight into how the synthesis conditions impact $MAPbI_3$ synthesis, a narrower, more refined screening FFD was necessary to explore the variables.

Refined screening design

Factor selection and design

After the initial screening FFD, a follow-on design was performed, looking at a smaller area of process space. Purification solvent polarity was removed as a factor as only the most non-polar solvents were suitable for purification. The purification solvent polarisability was retained as a factor since this affects down-stream processing such as ligand exchange and NC deposition, and so the impact on NC properties needs to be understood. Hexane, toluene and mesitylene were chosen as solvents with varying polarisability based on the solvent map.[39] The ligand concentration range was refined to avoid unsuccessful reactions. The non-polar solvent content and polarisability and ligand ratio ranges were identical to the initial screening design.

A five factor resolution V design was selected to investigate the factors which were highlighted as significant in the previous screening FFD design. The type of mixing junction was fixed throughout. The temperature was also fixed as a room temperature reaction was deemed most desirable. A summary of the factors and ranges are shown in Table 3, and the exact combination of experiments run is shown in Table 4. Nanocrystal solutions were prepared and PL spectra measured. As with the initial FFD screening experiments, the peak position, peak width and absolute peak intensity were measured as responses and the NC stability was noted.

Fractional factorial designs do not provide information on squared terms ($\beta_{ii}x_i^2$) but it is possible to see if a factor is having a non-linear effect on a response by the addition of an arbitrary squared term. Several models required a squared

Table 3 Optimisation design factors and ranges where −1, 0 and 1 are the low, centre and high values which are further explained in the ESI† Table S5

		Range		
	Factor	Low	Centre	High
1	Non-polar solvent/%	50	57.5	65
2	Non-polar solvent polarisability	−1	0	1
3	Ligand concentration (ligand : Pb)	6	8	10
4	Oleic acid/%	50	57.5	65
5	Purification solvent polarizability	−1	0	1

Table 4 Optimisation experimental design formulations and conditions

Exp no.	Run order	Non-polar solvent/%	Non-polar solvent	Ligand : Pb	Oleic acic/%	Purification solvent
N1	9	50	Hexane	6	50	Mesitylene
N2	1	65	Hexane	6	50	Hexane
N3	12	50	1-ODE	6	50	Hexane
N4	19	65	1-ODE	6	50	Mesitylene
N5	5	50	Hexane	10	50	Hexane
N6	6	65	Hexane	10	50	Mesitylene
N7	7	50	1-ODE	10	50	Mesitylene
N8	11	65	1-ODE	10	50	Hexane
N9	8	50	Hexane	6	65	Hexane
N10	13	65	Hexane	6	65	Mesitylene
N11	2	50	1-ODE	6	65	Mesitylene
N12	4	65	1-ODE	6	65	Hexane
N13	17	50	Hexane	10	65	Mesitylene
N14	14	65	Hexane	10	65	Hexane
N15	15	50	1-ODE	10	65	Hexane
N16	16	65	1-ODE	10	65	Mesitylene
N17	3	57.5	Dodecane	8	57.5	Toluene
N18	18	57.5	Dodecane	8	57.5	Toluene
N19	10	57.5	Dodecane	8	57.5	Toluene

term to describe the data and therefore nine additional experiments, Table 5, were performed to resolve the squared term.

Photoluminescence

All the refined screening experiments produced NCs. In addition, purifying the NCs in very non-polar solvents improved the colloidal stability of the product. 19 experiments were carried out. The chosen experimental conditions gave NCs with emission between 614 and 737 nm, Fig. 3b, indicating that the main PL emission peak could be tuned across a reasonable range for NCs made from a single perovskite material without the need for anion exchange. In addition, the control experiments N17–19 showed excellent reproducibility in the synthetic flow method. In the control experiments, the PL peak position for the unpurified product S1 was 725 nm ± 2 nm.

Once again two samples were collected, the first supernatant from centrifuging the reaction product (S1) and the second supernatant after resuspending the pellet in the purification solvent and centrifuging again (S2). A squared term was required to fit the model to the S1 peak position, S1 peak width, S1 peak intensity and S2 peak position. The squared term is required where there are non-linear responses to changes in the factors. Nine more complementary experiments, N20–28 (Table 5), were then run to allow us to fully resolve the unknown squared terms. These squared terms were found to be non-polar solvent content, non-polar solvent polarisability, and the ligand ratio (% oleic acid).

Analysis of the data, including the results of the 9 additional experiments, showed that models for S1 and S2 peak positions and the S1 peak intensity displayed high R^2 values (0.95, 0.97 and 0.95 respectively) and Q^2 values (0.86, 0.88 and 0.85 respectively) with excellent reproducibility (>0.97) indicating that the models were reliable. The S1 peak width model was satisfactory with lower R^2 and Q^2 values, 0.76 and 0.52 respectively, and high reproducibility (0.99). The metrics for the S2 width and S2 intensity indicated that the models were a poor fit and could not accurately describe the data. This is likely to be due to the purification step being uncontrolled which poorly accounts for the second supernatant peak width and intensity variation, possibly from osmotic swelling induced fragmentation of the NCs.[40]

The 4D contour plots shown in Fig. 4 allow the models to be clearly visualised. The response is shown by the colour gradient across two, three or, in this instance, four factors. Any additional model factors not displayed in the contour plot are typically set to their midpoint, but may be set to any value in the design space. In these plots, four factors are selected and the purification solvent polarisability is set to the mid point, toluene.

Fig. 4a and b show that to achieve a PL peak at shorter wavelengths requires high ligand ratio, low % OA, low reaction solvent ratio and a less polarizable reaction solvent (hexane). Whereas, for higher wavelength PL peaks a mid-high % OA, low ligand ratio, higher solvent content and more polarisable solvent (dodecane or 1-ODE) are required.

The models used to fit the PL peak width were satisfactory and poor for the S1 and S2 supernatants respectively. Fig. 4c

Table 5 Optimisation experimental design complementary experiments' formulations

Exp no.	Non-polar solvent/%	Non-polar solvent	Ligand : Pb/mmol : mmol	Oleic acic/%	Purification solvent
N20	50.0	Dodecane	8	57.5	Toluene
N21	65.0	Dodecane	8	57.5	Toluene
N22	57.5	Hexane	8	57.5	Toluene
N23	57.5	1-ODE	8	57.5	Toluene
N24	57.5	Dodecane	6	57.5	Toluene
N25	57.5	Dodecane	10	57.5	Toluene
N26	57.5	Dodecane	8	50.0	Toluene
N27	57.5	Dodecane	8	65.0	Toluene
N28	57.5	Dodecane	8	57.5	Toluene
N29	57.5	Dodecane	8	57.5	Hexane
N30	57.5	Dodecane	8	57.5	Mesitylene

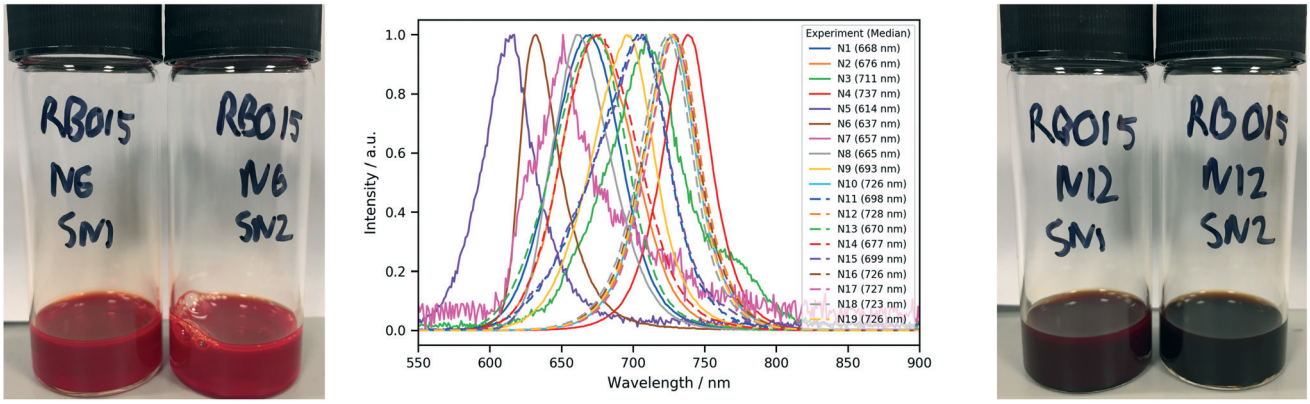

(a) N6 **(b)** S1 PL emission **(c)** N12

Fig. 3 Refined screening design (a) experiment N6, shortest PL wavelength, (b) S1 normalised PL emission response, and (c) experiment N12, longest PL wavelength NCs.

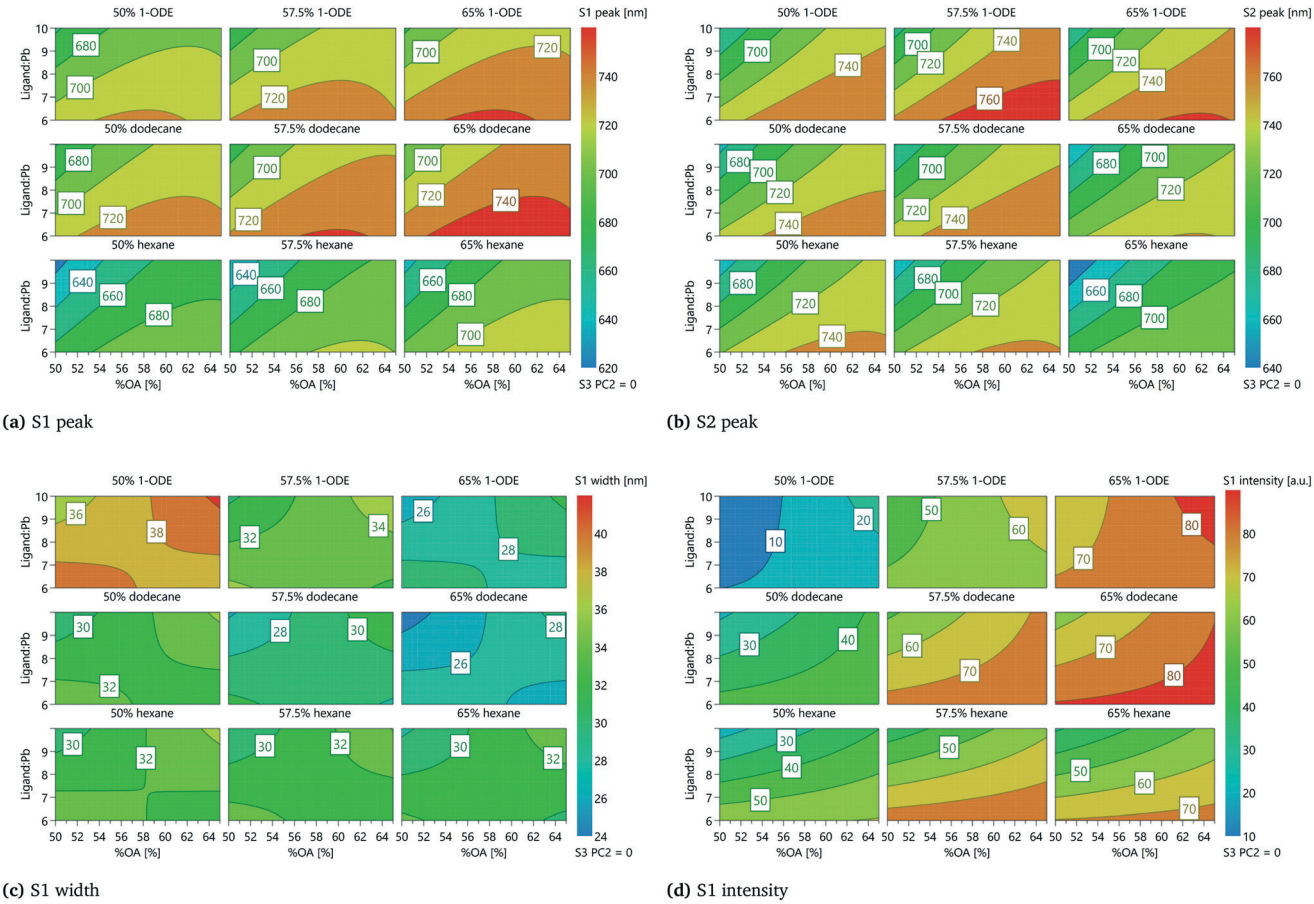

(a) S1 peak **(b)** S2 peak

(c) S1 width **(d)** S1 intensity

Fig. 4 Refined screening design 4D response contour plots for (a) S1 PL peak, (b) S2 PL peak, (c) S1 PL width, and (d) S1 PL intensity.

shows that high ligand concentration and 50% OA (top left corner of the subplots) produce NCs with a narrow S1 peak width. Under these conditions the PL peak is the most blue shifted, see Fig. 4a. This would be expected due to the decreasing size of the NCs. Meanwhile the opposite lower right shows low ligand concentration with high OA content, in this case the PL peaks have the lowest interquartile range and also have narrower peaks, possibly due to increased monodispersity.

The intensity of the S1 peak showed some additional general trends, as can be seen in Fig. 4d. The PL intensity was highest in the regions where the NCs were synthesized using lower ligand concentration, high % OA and greater non-polar solvent content. There is an interaction between

reaction solvent ratio and reaction solvent polarizability: at low solvent concentration, hexane gives a more intense peak and at high solvent concentration, dodecane and 1-ODE gave higher intensity peaks.

These results confirm observations from previous studies and extend them by providing insight into interactions and the effect of different solvents. Several studies have shown that increasing the ligand concentration has been shown to blue shift the PL emission for $CsPbBr_3$ and our results confirm this for $MAPbI_3$.[33,41,42] This study also supports studies where high OA : OLA ratio produced $MAPbI_3$ NCs with more red shifted PL emissions.[34] The interaction between ligand ratio and ligand concentration (the curved lines in Fig. 4) provide further insight into the effect of these factors. Though a narrower range of % non-polar reaction solvent was chosen compared to Fang *et al.*,[36] (due to the solubility of MAI in 1-butanol) our results showed a different trend to theirs with higher amounts of alcohol producing blue shifted PL emission in our experiments.[36] This is likely be due to the change in morphology from nanocubes to dots which will be discussed in the stability and morphology section. Finally the figures show the effect of different reaction solvents. While many studies use 1-ODE or hexane as the synthesis solvent, few have studied the impact of polarizability with only polarity having been investigated previously.[43] These results provide a more comprehensive insight into the variables which affect PL emission in alcohol based synthesis routes beyond the alcohol type and alcohol content which have been focused on previously.[36,44]

Stability and morphology

While the photoluminescence data provides insight into the optoelectronic properties of the NCs, the stability and morphology are also important. Since these are qualitative measurements, they can not be modelled using experimental design techniques and trends are more difficult to resolve. The complementary experiments, N20–N28, however allowed a clearer insight into the effect the chosen factors have on the stability and morphology.

In the S1 supernatant, 65% dodecane (N21) was more stable than 50% dodecane (N20), which is to be expected due to the lower amount of 1-butanol. Since the NCs are sensitive to polar solvent, increasing the polarity of the reaction solution by adding more butanol is likely to lower their stability. Non-polar solvent polarisability also had an impact on the S1 supernatant stability. Synthesis in 1-ODE (N23) led to a larger shift in the PL peak position with more bulk material being formed compared to hexane (N22). Lower ligand concentration supernatant, ligand : Pb = 6 (N24), was more stable than the higher ligand concentration, ligand : Pb = 10 (N25). The 50% OA (N26) S1 supernatant was less stable than 65% OA (N27). Once the pellet was resuspended in toluene (N28), the supernatant were stable over several months.

In Liang *et al.*'s study, control of the morphology was noted as being a key issue. $MAPbI_3$ NCs were observed as being cubic and $MAPbBr_3$ NCs were spherical. Analysing all 30 experiments using TEM would have been time consuming so therefore only N20–30 were studied, see ESI† Fig. S7 and S8.

The TEM images highlighted significant differences in the morphology. High non-polar solvent content (N21) led to spherical dots while the low non-polar solvent (N20) led to the formation of cubic NCs. Altering the synthesis solvent from hexane (N22) to 1-ODE (N23) changed the morphology from dots to cubic NCs. Increasing ligand concentration (N25) formed dots, while lower concentrations formed cubic NCs (N24). Most strikingly, 65% OA content (N27) formed cubic NCs while 50% OA formed a range of morphologies. Finally, the choice of purification solvent did not affect the NC shape but the clarity of the TEM images differed significantly. When preparing experiment N28, the sample were split into three centrifuge tubes and each pellet was redispersed in a different solvent. N29 purified in hexane appeared to contain more organic material in the TEM sample than N28 and N30 which was purified in toluene and mesitylene respectively. This organic material prevented us from obtaining clear TEM images of the NCs.

These results confirm previous observations of the impact of ligands on nanocrystal morphology and expands understanding further through solvent investigation Almeida *et al.* observed $CsPbBr_3$ nanocubes for low ligand concentrations and nanoplatelets for high ligand concentrations.[33] While nanoplatelets were not found, a morphology change was observed in changing the ligand concentration. Changing the ligand ratio has been widely reported to alter the morphology with high OA conditions tending to favour nanocubes, as was observed here.[45–47] In the Fang *et al.* study which investigated alcohol content, increased amounts of alcohol red shifted the PL emission, however, no TEM images were reported for these results.[36] Furthermore, the morphological impact of the halide ratio and OA *vs.* IPA were reported with a range of morphologies being observed for different halides and using OA instead of IPA favoured non-oriented crystal growth (nanocubes). In the investigation of non-polar solvent polarity by Dutta *et al.*,[43] more polar solvents favoured orthorhombic $CsPbBr_3$ and $CsPbCl_3$ nanocubes, while the non-polar solvents were trigonal Cs_4PbBr_6 and $CsPbCl_3$ nanoplatelets.[43] Solvent polarizability was not investigated in their study and our results provide further insight into solvent engineering, and increased clarity on the multiple factors that influence morphology.

Validation

After concluding the complementary experiments and producing the models for all the responses, model validation was necessary to verify the models were correct and able to accurately predict the experimental conditions needed to produce a peak at a specified wavelength. To validate the model, seven target wavelengths from 620–740 nm, at 20 nm intervals, were specified and the model was instructed to minimise the peak width. Solvents were specified as hexane

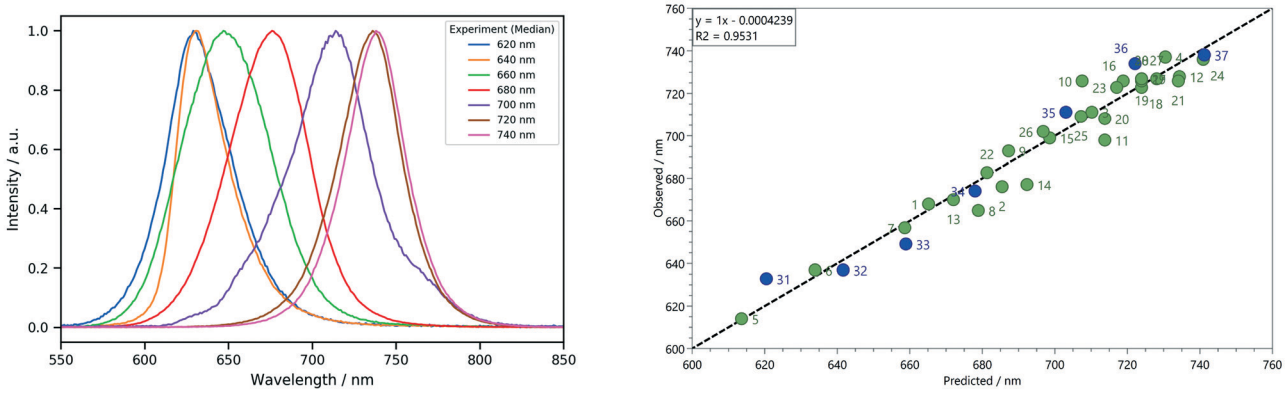

(a) S1 normalised PL emission **(b)** Observed vs predicted PL response

Fig. 5 S1 peak model validation experiment (a) S1 normalised PL emission, and (b) observed *vs.* predicted wavelength PL centred on, showing design experiments in green and validation experiments in blue.

for 620–680 nm and 1-ODE for 700–740 nm to simplify the precursor preparation. The model equations were used to generate predicted experimental conditions for target emission wavelengths, as shown in the ESI† Table S8. The predicted and observed data were then compared (Fig. 5), which established the validity of the models.

The observed results match the predicted values well and fall within two standard deviations and are therefore statistically valid. This study highlights the potential of experimental design to predict the experimental conditions needed to produce NCs with PL at a specified wavelength.

Some aspects of the DoE studies and validation results should be generalisable to other perovskite materials as the effect of temperature and ligand concentration on PL emission have been observed in other one variable at a time studies,[6,21,33,34] however not all of the results may be transferred so easily to other perovskite materials, ligands, or synthesis routes. For example, Fang *et al.* observed various morphologies depending on the halide ratio when using alcohols to synthesise $CsPbX_3$ and when changing the solvent polarity Dutta *et al.*[43] observed a shape change in $CsPbCl_3$ and a phase change in $CsPbBr_3$.[36,43] Li *et al.* investigated synthesising $CsPbBr_3$ NCs using various C8 ligands and did not observe the same PL emission trend as we did when changing the OA : OLA ratio. Altering the ligand ratio had little effect on the PL emission peak position in their study, with temperature being the more significant factor over the ranges studied.[48] Perovskite NC materials therefore behave differently depending on the specific surface chemistry between the material and the ligands used, and alcohol-based perovskite NC synthesis is still relatively novel.[36,44,49] DoE should ideally be repeated for hot injection, ligand assisted reprecipitation, and heat up methods such as microwave synthesis, as well as for other materials such as $CsPbrBsPbBr_3$ or novel lead-free perovskite materials.[50–52] This study provides greater insight into the alcohol based perovskite NC synthesis and could be extended to investigate other responses such as degradation or optoelectronic device performance.[53,54]

Conclusions

In summary, in the synthesis of $MAPbI_3$, eight factors were screened using design of experiments to identify the most significant variables. The factors screened were the ligand concentration, ligand ratio, purification solvent polarizability, purification solvent polarity, non-polar solvent ratio, non-polar solvent polarizability, temperature, and mixing T-junction. The key factors which influenced NC properties within the ranges studied were the ligand concentration, ligand ratio, purification solvent polarizability, non-polar solvent ratio, and the non-polar solvent polarizability. Once these factors had been identified, a more refined screening was performed to model the data using multiple linear regression. The model was then successfully validated by choosing conditions which were selected to produce NCs with PL peaks at 20 nm intervals while minimising the peak width. The model showed an excellent agreement between the observed and the predicted PL emission peak position. Besides the PL properties, insight was also gained into how the factors affect the NC stability and morphology. Design of experiments proved to be an efficient method to screen many more factors than is traditionally investigated in the literature and would be suited to investigate the synthesis of other materials or processes.

Conflicts of interest

There are no conflicts to declare.

Acknowledgements

This work was supported by the Engineering and Physical Sciences Research Council EP/L016354/1 at the ESPRC Centre for Doctoral Training in Sustainable Chemical Technologies, University of Bath. The authors acknowledge the University of Bath for providing access to the fluorimeter and UV-vis spectrometer, and Dr Philip Fletcher and Dr Gabriele Kociok-Kohn in the Material and Chemical Characterisation Facility for their assistance in TEM and XRD acquisition.

References

1 M. M. Lee, J. Teuscher, T. Miyasaka, T. N. Murakami and H. J. Snaith, *Science*, 2012, **338**, 643–647.
2 National Renewable Energy Laboratory NREL, Best Research-Cell Efficiencies, 2021, https://www.nrel.gov/pv/cell-efficiency.html.
3 Z.-K. Tan, R. S. Moghaddam, M. L. Lai, P. Docampo, R. Higler, F. Deschler, M. Price, A. Sadhanala, L. M. Pazos, D. Credgington, F. Hanusch, T. Bein, H. J. Snaith and R. H. Friend, *Nat. Nanotechnol.*, 2014, **9**, 687–692.
4 G. Xing, N. Mathews, S. S. Lim, N. Yantara, X. Liu, D. Sabba, M. Grätzel, S. Mhaisalkar and T. C. Sum, *Nat. Mater.*, 2014, **13**, 476–480.
5 L. Dou, Y. M. Yang, J. You, Z. Hong, W. H. Chang, G. Li and Y. Yang, *Nat. Commun.*, 2014, **5**, 1–6.
6 L. Protesescu, S. Yakunin, M. I. Bodnarchuk, F. Krieg, R. Caputo, C. H. Hendon, R. X. Yang, A. Walsh and M. V. Kovalenko, *Nano Lett.*, 2015, **15**, 3692–3696.
7 Q. A. Akkerman, V. D'Innocenzo, S. Accornero, A. Scarpellini, A. Petrozza, M. Prato and L. Manna, *J. Am. Chem. Soc.*, 2015, **137**, 10276–10281.
8 G. Nedelcu, L. Protesescu, S. Yakunin, M. I. Bodnarchuk, M. J. Grotevent and M. V. Kovalenko, *Nano Lett.*, 2015, **15**, 5635–5640.
9 A. Swarnkar, R. Chulliyil, V. K. Ravi, M. Irfanullah, A. Chowdhury and A. Nag, *Angew. Chem., Int. Ed.*, 2015, **54**, 15424–15428.
10 G. Niu, A. Ruditskiy, M. Vara and Y. Xia, *Chem. Soc. Rev.*, 2015, **44**, 5806–5820.
11 J. Jean, J. Xiao, R. Nick, N. Moody, M. Nasilowski, M. Bawendi and V. Bulović, *Energy Environ. Sci.*, 2018, **11**, 2295–2305.
12 F. Zhang, H. Zhong, C. Chen, X.-G. Wu, X. Hu, H. Huang, J. Han, B. Zou and Y. Dong, *ACS Nano*, 2015, **9**, 4533–4542.
13 S. Wei, Y. Yang, X. Kang, L. Wang, L. Huang and D. Pan, *Chem. Commun.*, 2016, **52**, 7265–7268.
14 X. Li, Y. Wu, S. Zhang, B. Cai, Y. Gu, J. Song and H. Zeng, *Adv. Funct. Mater.*, 2016, **26**, 2435–2445.
15 I. Lignos, S. Stavrakis, G. Nedelcu, L. Protesescu, A. J. Demello and M. V. Kovalenko, *Nano Lett.*, 2016, **16**, 1869–1877.
16 I. Lignos, R. Maceiczyk and A. J. DeMello, *Acc. Chem. Res.*, 2017, **50**, 1248–1257.
17 R. M. Maceiczyk, K. Dümbgen, I. Lignos, L. Protesescu, M. V. Kovalenko and A. J. DeMello, *Chem. Mater.*, 2017, **29**, 8433–8439.
18 I. Lignos, V. Morad, Y. Shynkarenko, C. Bernasconi, R. M. Maceiczyk, L. Protesescu, F. Bertolotti, S. Kumar, S. T. Ochsenbein, N. Masciocchi, A. Guagliardi, C. J. Shih, M. I. Bodnarchuk, A. J. Demello and M. V. Kovalenko, *ACS Nano*, 2018, **12**, 5504–5517.
19 I. Lignos, L. Protesescu, D. B. Emiroglu, R. MacEiczyk, S. Schneider, M. V. Kovalenko and A. J. DeMello, *Nano Lett.*, 2018, **18**, 1246–1252.
20 X. Liang, R. W. Baker, K. Wu, W. Deng, D. Ferdani, P. S. Kubiak, F. Marken, L. Torrente-Murciano and P. J. Cameron, *React. Chem. Eng.*, 2018, **3**, 640–644.
21 H. Huang, A. S. Susha, S. V. Kershaw, T. F. Hung and A. L. Rogach, *Adv. Sci.*, 2015, **2**, 1500194.
22 J. Song, J. Li, X. Li, L. Xu, Y. Dong and H. Zeng, *Adv. Mater.*, 2015, **27**, 7162–7167.
23 A. Pan, B. He, X. Fan, Z. Liu, J. J. Urban, A. P. Alivisatos, L. He and Y. Liu, *ACS Nano*, 2016, **10**, 7943–7954.
24 S. Sun, D. Yuan, Y. Xu, A. Wang and Z. Deng, *ACS Nano*, 2016, **10**, 3648–3657.
25 S. Costanzo, G. Simon, J. Richardi, P. Colomban and I. Lisiecki, *J. Phys. Chem. C*, 2016, **120**, 22054–22061.
26 F. Zhang, S. Huang, P. Wang, X. Chen, S. Zhao, Y. Dong and H. Zhong, *Chem. Mater.*, 2017, **29**, 3793–3799.
27 L. Bezinge, R. M. Maceiczyk, I. Lignos, M. V. Kovalenko and A. J. Demello, *ACS Appl. Mater. Interfaces*, 2018, **10**, 18869–18878.
28 D. B. Hibbert, *J. Chromatogr. B: Anal. Technol. Biomed. Life Sci.*, 2012, **910**, 2–13.
29 P. K. Sahu, N. R. Ramisetti, T. Cecchi, S. Swain, C. S. Patro and J. Panda, *J. Pharm. Biomed. Anal.*, 2018, **147**, 590–611.
30 A. Ariyarit, I. Takenaka, R. Yoshikawa, F. Gillot and S. Shiratori, *RSC Adv.*, 2016, **6**, 98052–98058.
31 L. Li, N. Liu, Z. Xu, Q. Chen, X. Wang and H. Zhou, *ACS Nano*, 2017, **11**, 8804–8813.
32 S. Galliano, F. Bella, G. Piana, G. Giacona, G. Viscardi, C. Gerbaldi, M. Grätzel and C. Barolo, *Sol. Energy*, 2018, **163**, 251–255.
33 G. Almeida, L. Goldoni, Q. Akkerman, Z. Dang, A. H. Khan, S. Marras, I. Moreels and L. Manna, *ACS Nano*, 2018, **12**, 1704–1711.
34 I. Levchuk, P. Herre, M. Brandl, A. Osvet, R. Hock, W. Peukert, P. Schweizer, E. Spiecker, M. Batentschuk and C. J. Brabec, *Chem. Commun.*, 2017, **53**, 244–247.
35 L. Yuan, R. Patterson, X. Wen, Z. Zhang, G. Conibeer and S. Huang, *J. Colloid Interface Sci.*, 2017, **504**, 586–592.
36 F. Fang, W. Chen, Y. Li, H. Liu, M. Mei, R. Zhang, J. Hao, M. Mikita, W. Cao, R. Pan, K. Wang and X. W. Sun, *Adv. Funct. Mater.*, 2018, **28**, 1–10.
37 C. M. Alder, J. D. Hayler, R. K. Henderson, A. M. Redman, L. Shukla, L. E. Shuster and H. F. Sneddon, *Green Chem.*, 2016, **18**, 3879–3890.
38 R. Wu, Y. Yang, M. Li, D. Qin, Y. Zhang and L. Hou, *Nanomaterials*, 2017, **7**, 201.
39 P. M. Murray, F. Bellany, L. Benhamou, D.-K. Bučar, A. B. Tabor and T. D. Sheppard, *Org. Biomol. Chem.*, 2016, **14**, 2373–2384.
40 Y. Tong, F. Ehrat, W. Vanderlinden, C. Cardenas-Daw, J. K. Stolarczyk, L. Polavarapu and A. S. Urban, *ACS Nano*, 2016, **10**, 10936–10944.
41 R. Grisorio, E. Fanizza, I. Allegretta, D. Altamura, M. Striccoli, R. Terzano, C. Giannini, V. Vergaro, G. Ciccarella, N. Margiotta and G. P. Suranna, *Nanoscale*, 2020, **12**, 623–637.

42 A. Dutta, S. K. Dutta, S. Das Adhikari and N. Pradhan, *ACS Energy Lett.*, 2018, **3**, 329–334.
43 A. Dutta, R. K. Behera and N. Pradhan, *ACS Energy Lett.*, 2019, **4**, 926–932.
44 Y. Li, H. Huang, Y. Xiong, A. F. Richter, S. V. Kershaw, J. Feldmann and A. L. Rogach, *ACS Nano*, 2019, **13**, 8237–8245.
45 Z. Liang, S. Zhao, Z. Xu, B. Qiao, P. Song, D. Gao and X. Xu, *ACS Appl. Mater. Interfaces*, 2016, **8**, 28824–28830.
46 W. Liu, J. Zheng, S. Cao, L. Wang, F. Gao, K. C. Chou, X. Hou and W. Yang, *Inorg. Chem.*, 2018, **57**, 1598–1603.
47 O. Vybornyi, S. Yakunin and M. V. Kovalenko, *Nanoscale*, 2016, **8**, 6278–6283.
48 S. Li, R. W. Baker, I. Lignos, Z. Yang, S. Stavrakis, P. D. Howes and A. J. Demello, *Mol. Syst. Des. Eng.*, 2020, **5**, 1118–1130.
49 J. Cheng, S. Yuan, L. Zhu, L. Chen, C. Liu, H. Tong and H. Zeng, *Langmuir*, 2020, **36**, 3565–3572.
50 J. Huang, T. Lei, M. Siron, Y. Zhang, S. Yu, F. Seeler, A. Dehestani, L. N. Quan, K. Schierle-Arndt and P. Yang, *Nano Lett.*, 2020, **20**, 3734–3739.
51 L. Zhou, J. F. Liao, Z. G. Huang, X. D. Wang, Y. F. Xu, H. Y. Chen, D. B. Kuang and C. Y. Su, *ACS Energy Lett.*, 2018, **3**, 2613–2619.
52 B. J. Moon, S. J. Kim, S. Lee, A. Lee, H. Lee, D. S. Lee, T. W. Kim, S. K. Lee, S. Bae and S. H. Lee, *Adv. Mater.*, 2019, **1901716**, 1–7.
53 B. McKenna, A. Shivkumar, B. Charles and R. C. Evans, *Nanoscale*, 2020, **12**, 11694–11702.
54 B. Cao, L. A. Adutwum, A. O. Oliynyk, E. J. Luber, B. C. Olsen, A. Mar and J. M. Buriak, *ACS Nano*, 2018, **12**, 7434–7444.